Trap Level Measurements in Wide Band Gap Materials by Thermoluminescence

Pooneh Saadatkia, Chris Varney and Farida Selim

Additional information is available at the end of the chapter

Abstract

The electrical and optical properties of wide band gap materials are greatly affected by the presence of defects in the band gap. Identification and characterization of these defects that act as electron and hole traps are essential to understand charge carrier and exciton dynamics and ultimately control the electrical and optical properties of dielectrics and semiconductors. In this chapter, we will demonstrate how thermoluminescence (TL) spectroscopy can be used to characterize traps and measure their energy levels in the band gap. An advanced wavelength-based TL spectrometer will be presented, and its applications for the evaluation of trap levels and the characterization of donors and acceptors in semiconductors and dielectrics will be discussed.

Keywords: dielectrics and semiconductors, wide band gap materials, trap levels, exciton dynamics, luminescence

1. Introduction

The electrical and optical properties of materials are greatly affected by the presence of deep and shallow traps in the band gap. Deep traps capture charge carriers and prevent their recombination while shallow traps affect the transport of charge carriers and excitons in the lattice. Thus, identification and characterization of the electron and hole traps are essential to understand exciton and charge carrier dynamics and ultimately control the electrical and optical properties of dielectrics and semiconductors. Thermoluminescence (TL) spectroscopy can offer a powerful tool for the study of traps and the measurement of their depth in the band gap. It is commonly used for dosimetry and has also been applied for defect investigation and radiation damage studies. Recently, we have developed an advanced wavelength-based TL spectrometer for the evaluation of trap levels and the characterization of donors and acceptors and employed it to study a number of semiconductors and dielectrics.

INTECH

open science | open minds

This chapter explains in detail the basics of TL spectroscopy and introduces the reader to its use an effective method for trap and donor and acceptor characterization. Then it describes the experimental details of an advanced TL spectrometer, explains how to construct TL glow curves, and discusses different approaches for the calculations of trap levels in the band gap. The chapter also discusses in brief some of the complimentary methods that can be used in parallel with TL for the full characterization of traps including their structure, type, density, and energy level. Examples of these methods include positron annihilation and optical absorption spectroscopies. A few TL studies of traps in semiconductors and dielectrics are presented.

The chapter is organized as follows. It begins in Section 2 with a historical background about TL and its applications to radiation dosimetry and defect studies then it discusses the TL process and physics in Section 3. Section 4 gives a complete analysis for activation energy and trap level calculations including initial rise method, different heating rate method for first-order kinetics, and finally, it describes an analysis of general order kinetics. In Section 5, we describe the standard TL setup "TL reader", then introduce our advanced TL spectrometer that is especially useful for the study of traps in dielectrics and the characterization of donors and acceptors in semiconductors. Sections 6 and 7 discuss in detail the application of TL in the study of wide band gap materials by presenting our recent studies on yttrium aluminum garnet (YAG) as an example of dielectrics and ZnO as an example of wide band gap semiconductors.

2. Historical background

In Latin "lumen" means light, the term "luminescent" materials refer to materials that can emit light, especially in the visible range such as crystals, minerals, and chemical substances. Luminescence phenomena have been known for long times [1], it does not occur spontaneously, it needs some source of energy such as visible light, ultraviolet light, or X-rays in order to excite the sample [2]. Cascariolo [3] made the first attempt to create luminescence artificially from Bolognian stone in 1603. Afterwards, the stone and other luminescent materials were named "phosphor". In 1852, Stokes [4] formulated luminescence law, the energy of emission is typically less than the energy of absorption; therefore, luminescence occurs at lower energies or longer wavelengths. Later in 1888, Weidemann [5] used the term "luminescenz" for all phenomena of light not produced through increased temperature, i.e., incandescence. Luminescence is classified to many types such as photoluminescence, cathodoluminescence, thermoluminescence, and X-ray luminescence [6, 7].

Measuring material properties as a function of temperature is called thermally stimulated processes (TSPs) that are usually as follows: first, the sample is perturbed, in most cases by exposure to some source of ionizing radiation, then by elevating the temperature, it is thermally stimulated back to equilibrium that releases accumulated energy as light emission in TL or as current in thermally stimulated conductivity [8]. We will limit our discussion and literature review in this chapter to TL spectroscopy. Existence of thermoluminescence in crystals is dependent on the presence of crystal defects that are capable of absorbing some part of incident energy during irradiation, and only emit light after heating the material [9–13].

Different types of irradiation sources can be used to excite the samples in TL measurement such as γ-rays, X-rays, and UV radiation. The dependence of energy absorbed during irradiation, which is termed "radiation dose" and defined as dose rate × time of exposure makes TL very effective in radiation dosimetric applications [14, 15] in medicine, industry, biology and agriculture, and also in dating of ancient pottery sherds and certain rocks [16, 17]. Besides dosimetric applications, thermoluminescence spectroscopy is a versatile tool for defect studies in crystals and trapping phenomena at the grain boundaries in nanostructures and soft materials.

The TL glow curve represents the intensity of emitted light versus temperature; each glow peak is associated with recombination center and related to specific trap. Activation energy and escape frequency factor can be calculated from the glow curve [18]. As mentioned in the introduction, TL is an important technique for investigating of nature and depth of traps in the different type of solids [19, 20], and various methods can be used to calculate trap parameters based on the kinetics order of glow peaks such as initial rise method and variable heating rates that will be discussed later. Heating rate has critical effect on the intensity and peak area of thermoluminescence glow peaks [21]. Variable heating rate techniques including very slow heating rate down to 0.0008°C/s were used to investigate the TL of CaSO$_4$: Tm phosphor. Using slow heating rates helped to resolve eight narrow components in the TL glow curve [22]. Because of inner shell electronic transitions, rare-earth ions and transition metal ions are considered excellent luminescence centers [23–28]. For example, TL measurement was applied to investigate the luminescence efficiency of rare-earth ions doped SrTiO$_3$:Pr^{3+} [28]. The authors used a 100 W deuterium lamp for excitation and measured emission from as-fired SrTiO$_3$:Pr^{3+} and annealed samples in reduced atmosphere (5% H$_2$ and 95% Ar). They observed a considerable decrease in the TL intensity of the annealed samples, which were attributed to the suppression of traps. They also tried to increase the luminescence efficiency of SrtiO$_3$:Pr^{3+} by adding impurities. After adding Al, new peaks were appeared, it seems that above 150 k, Al^{3+} ions are responsible for providing free carriers, which help to improve the luminescence efficiency of Pr^{3+} [28].

Recently, nanosized phosphor has fascinated researchers, and its applications have been emerged in different fields of materials especially luminescence area [29]. They have great potential for high dose detection in dosimetry applications [30, 31]. ZrO$_2$ nanophosphor is a good example where TL spectroscopy was successfully applied to study its properties [30]. Different concentrations of titanium were used as dopants to study TL behavior of ZrO$_2$ nanophosphors [32]. Samples were exposed to 254 nm UV for variable times in order to study the effect of time exposure and dose on TL intensity. Trapping parameters, i.e., activation energy and frequency factor were also calculated with different heating rate and peak shape methods. By increasing the heating rate, peaks position were shifted to higher temperature side. The sample was found to be useful for TL dosimetry applications due to linear dose response, high stability, and low fading phenomenon. Two peaks were observed at 167 and 376°C with fixed positions, and enhancing or quenching of intensity was found to be strongly dependent on dopant concentrations. Similarly, Tamrakar et al. [33] used TL spectroscopy to study the effect of different concentration of Er^{3+} as dopant for gadolinium oxide nanophosphor (Gd$_2$O$_3$:Er^{3+} phosphor). They found shallow and deep traps when using

254 nm UV irradiation and Co^{60} gamma irradiation, respectively. In addition, gamma-irradiated samples indicated low fading and higher stability in comparison with samples exposed to UV. However, UV-irradiated Mn-doped $CaYAl_3O_7$ phosphor indicates higher intensity compared to the samples irradiated by Gamma and megavoltage beam, indicating that by exposing to lower energy radiations, large numbers of shallower traps were formed [34]. Gamma rays have also been applied to irradiate pure LiF crystals to investigate trap levels and their connections to color centers generated during ionization process. The authors reported the relation of four color centers to four resolved and six unresolved glow peaks, which shows that TL spectroscopy is quite useful [35].

It is important to mention that the physical and optical properties of individual nanosize phosphor materials are often not the same as those of their bulk counterparts [36–39]. For example, activation energy and trap parameters were calculated by Tamrakar et al. [37, 40] from TL glow curve of bulk CdS and CdS: Cu phosphor nanoparticles using Chen's peak shape methods [8, 41–43]. The former was found to exhibit first-order kinetics while the second one showed general order kinetics in TL emission implying the presence of charge retrapping in the nanoparticles. They also found that the level of excitation, presence of other traps, and preionized luminescence centers can affect the shape, intensity, and position of a glow curve.

3. Basics of TL process

In a typical TL measurement, a sample is irradiated with high-energy light for a duration, which excites electrons from the valence band or from the dopant levels within the band gap to the conduction band. The excited state is not stable, so after some time the charge carriers recombine. A fraction of charge carriers may be trapped at a defect or impurity and cannot recombine with their counterpart. After removal of the excitation, heating injects thermal energy into the system, providing the trapped charge carriers with the energy necessary to escape their traps. These released charge carriers can either recombine with their charge carrier counterpart at luminescence centers, giving rise to TL emission, or they can become trapped at a deeper, higher-energy trap. They possess too much energy at this point to retrap at the same type of trap they just escaped or any shallower trap. The probability of detrapping increases with raising temperature. **Figure 1** presents a schematic diagram of the process of thermal stimulation and recombination of trapped charge carriers. TL emission intrinsically occurs at one or few luminescence centers. Thus, TL measurements provide a reliable method by which to record small luminescence intensities. This makes TL an ideal method for the characterization of trap levels in insulating crystals such as yttrium aluminum garnet ($Y_3Al_5O_{12}$) [44–58].

4. Activation energy and trap level calculations

A plot of thermoluminescence intensity versus temperature is known as a glow curve. Analysis of glow curves can provide quantitative information about trap levels. Most notably, one may use glow curve analysis to calculate the depth of the charge carrier traps. The calculated
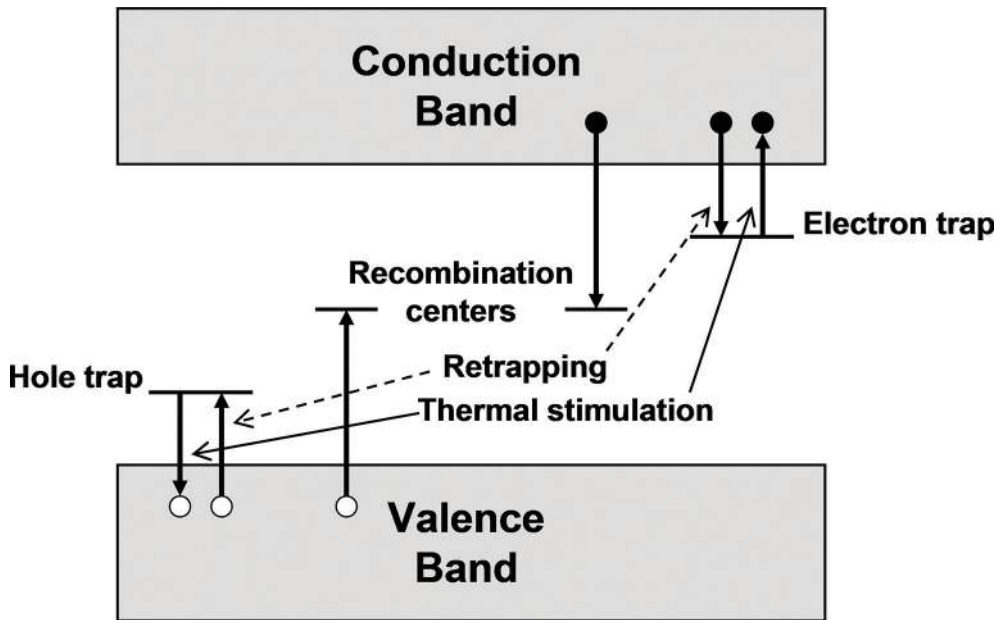
Figure 1. Schematic diagram of the TL process after the thermal activation of trapped charge carriers [55].

depth of a trap is referred to as its activation energy. To explain TL phenomena, Randall and Wilkins presented a model based on a single defect level within the band gap and assumed negligible retrapping, in which case the charge carrier can go straight to a luminescence center [59–61]. This is based on first-order kinetics of TL. Higher order kinetics assumes higher degrees of retrapping.

There are several methods to calculate activation energy from glow curves based on TL kinetics. The initial rise method calculates the activation energy directly by fitting the beginning of TL peak and is applicable to any order kinetics but can only be applied for nonoverlapping glow curves, where the peak being studied initially rises from the baseline [2, 41, 55, 62–64]. Other methods of activation energy calculation rely on conducting the experiment multiple times with different heating rates. At a faster heating rate, a glow curve shifts to higher temperature [2, 41, 65]. This effect is shown in **Figure 2** for glow curves of YAG doped with Ce to 0.2% concentration (Ce:YAG 0.2%) at heating rates of 5, 10, 20, 30, 40, 50 and 60°C/min. The method of two heating rates uses two separate constant heating rates to cancel unknown terms in kinetics calculations, thus rendering activation energy calculation trivial [2, 41, 55, 65–66]. This method is limited by peak fitting capabilities, and since peak temperature is usually not very sensitive to the heating rate, can give large uncertainty.

This method is typically applied to first-order kinetics, but it is possible to apply this method to any order kinetics. Following the same principles as the method of two heating rates is the variable heating rate method, where several glow curves using different heating rates are constructed [2, 55]. As with the method of two heating rates, unknown terms cancel in kinetics
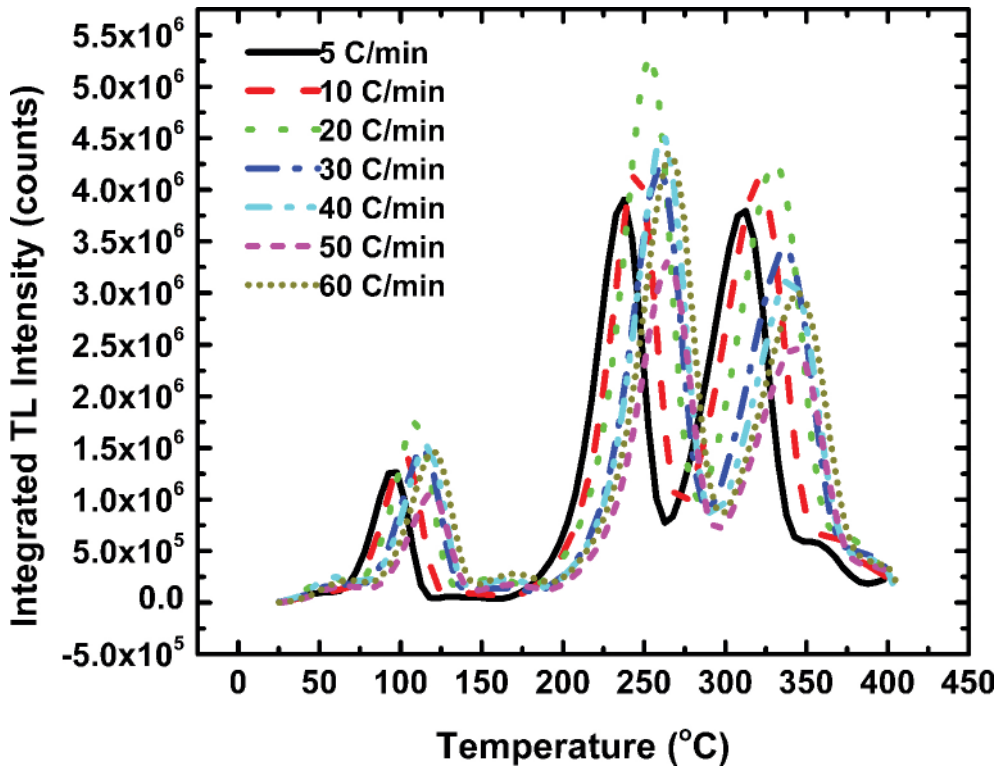
Figure 2. Glow curves of Ce:YAG 0.2% at multiple heating rates, showing the effects of heating rate on glow curve peaks.

equations, and in this case the activation energy can be determined graphically. The benefit of this method over the method of two heating rates is that the greater number of data points decreases uncertainty. This method is typically applied to first-order kinetics, but it can be generalized to any order kinetics. Other methods, such as the half-width method or direct computational glow curve fitting with the activation energy as a fitting parameter, are not explored in this chapter.

4.1. Initial rise method

Let us now derive each of the discussed methods for determining activation energies. The probability p of an electron escaping from a trap of depth at temperature T can be described by the Arrhenius Equations [60, 65, 67].

$$p = s\exp\left(-\frac{E}{k_B T}\right) \qquad (1)$$

where k_B is the Boltzmann constant and s, known as the frequency factor, is given by [67]

$$s = N_B v \sigma_t \tag{2}$$

where N_B is the density of states in the band in which the carriers escape, v is the carrier's thermal velocity, and σ_t is the trap's capture cross section. The frequency factor s has units of time^{-1} and may vary weakly with temperature. The rate of detrapping $-dn/dt$ at temperature T can be expressed as

$$-\frac{dn}{dt} = s\, n\, \exp\left(-\frac{E}{k_B T}\right) \tag{3}$$

where n is the concentration of trapped charge carriers. Determining $n(T)$ follows from Eq. (3) by

$$\frac{dn}{n} = -s\, \exp\left(-\frac{E}{k_B T}\right) dt = -\frac{s}{q}\, \exp\left(-\frac{E}{k_B T}\right) dT \tag{4}$$

where $q = dT/dt$ is the heating rate, which for simplicity we shall assume is linear. Integration gives

$$\ln(n) = -\int \frac{s}{q}\, \exp\left(-\frac{E}{k_B T'}\right) dT' + \text{constant} \tag{5}$$

The prime in T' is introduced to distinguish between the variable and the upper limit of integration. When $t = 0$, let $n = n_0$ and $T = T_i =$ some initial temperature, then the constant is equal to n_0 and we have

$$\ln\left(\frac{n}{n_0}\right) = -\int_{T_i}^{T} \frac{s}{q} \exp\left(-\frac{E}{k_B T'}\right) dT'$$
or
$$n = n_0 \exp\left[-\int_{T_i}^{T} \frac{s}{q} \exp\left(-\frac{E}{k_B T'}\right) dT'\right] \tag{6}$$

The thermoluminescence intensity I is proportional to the rate that charge carriers are supplied to luminescence centers [2, 41, 60, 64–65, 68–69]:

$$I(T) = -c\frac{dn}{dt}$$
$$= c\, s\, n \exp\left(-\frac{E}{k_B T}\right). \tag{7}$$

Combining this with Eq. (6),

$$I(T) = c\, s\, n_0 \exp\left(-\frac{E}{k_B T}\right) \exp\left[-\int_{T_i}^{T} \frac{s}{q} \exp\left(-\frac{E}{k_B T'}\right) dT'\right] \tag{8}$$

which is known as the Randall-Wilkins first-order expression of a single glow peak [60]. For low temperatures ($T \approx T_i$), we may estimate $n \approx n_0$ and thus write

$$I \approx c \, s \, n_0 \exp\left(-\frac{E}{k_B T}\right) \tag{9}$$

The initial rise method, introduced by Garlick and Gibson [64], is based on Eq. (9). To calculate the activation energy by the initial rise method, we may rewrite Eq. (9) in a more useful form

$$\ln(I) = \ln(c \, s \, n_0) - \frac{E}{k_B T} \tag{10}$$

Plotting $\ln(I)$ versus $1/k_B T$ gives the slope $= E$.

The initial rise method is applicable to first, second, and even general order cases, but it is limited to the region where $I_i \leq I \ll I_m$.

Bräunlich [62] showed that the values found for E using the initial rise method will be smaller than the actual values when the retrapping factor $R[h(T_i)/f(T_i)] \gg 1$, where R is given by

$$R = \frac{\text{probability of retrapping}}{\text{probability of recombination}} \tag{11}$$

and $h(T_i)$ and $f(T_i)$ are traps with electrons and the initial concentration of unoccupied recombination centers, respectively (at the temperature T_i). This suggests that the initial rise method actually gives a poor estimate for E for high order kinetics.

Christodoulides [63] estimated a correction to the initial rise method that may be used if the intensity of the range used for calculation is larger than a small fraction of the peak height. The activation energy calculated by the initial rise method EIR can be adjusted to the corrected value of the activation energy E_C by

$$E_C = (1 + 0.74a_1 + 0.082a_2)E_{IR} - (2a_1 + 0.22a_2)\frac{T_m}{11,605} \tag{12}$$

The factors a_1 and a_2 are the fraction of the peak value of the TL intensity observed at temperatures T_1 and T_2, respectively, marked as the lower and upper bounds of the fit, as demonstrated in **Figure 3**.

4.2. Methods of variable heating rates

The initial rise method is applicable to general order kinetics, but with decreased accuracy for higher order kinetics. However, if peaks are overlapped it is not possible to apply this method since the beginning of a peak is not available for analysis. The methods of two and variable heating rates only require that the peak temperature can be determined for calculation of E. These methods can be used with general order kinetics. The methods of two and variable heating rates can be derived from first-order kinetics or simplified from general order kinetics. We will first derive the method for general order kinetics and then apply it to the case of
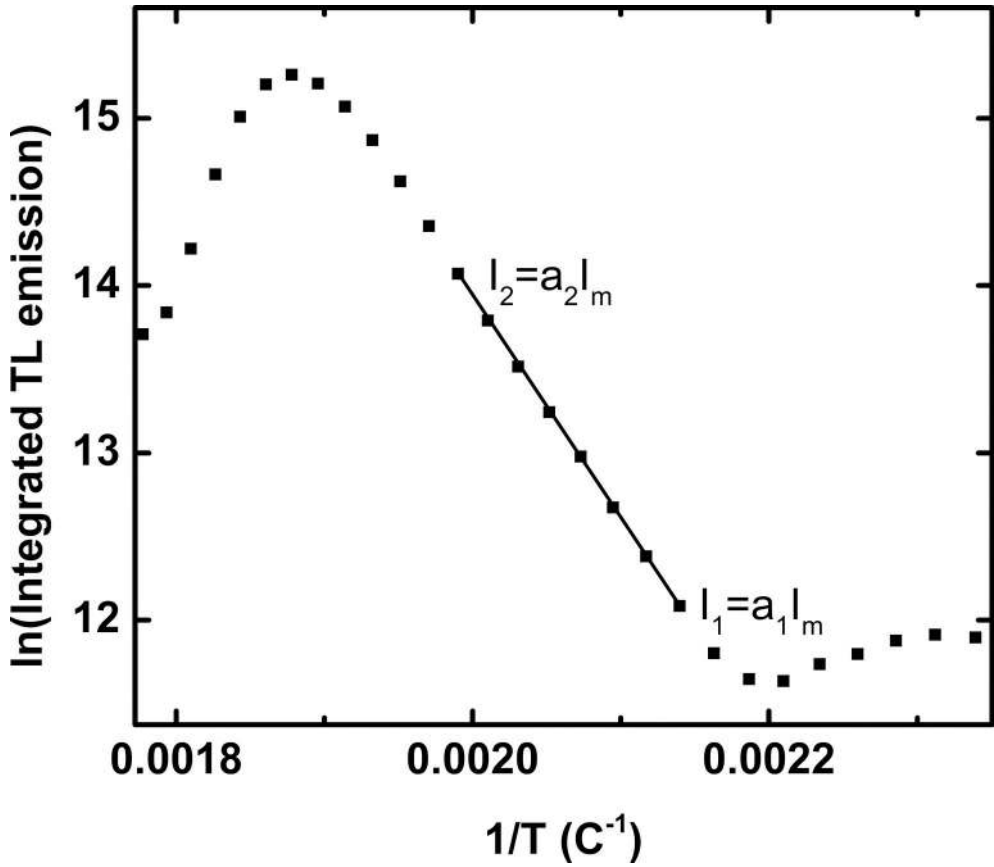
Figure 3. TL glow curve of Ce:YAG 0.2% plotted as ln(I) versus 1/T for calculation of the activation energy by the initial rise method, demonstrating the definitions of a_1 and a_2.

first-order kinetics. It will be necessary to assume that s is independent of temperature to proceed with this derivation. To general order of kinetics, Eq. (7) becomes [2, 41, 65, 69–71]

$$I(T) = -c\frac{dn}{dt} = c\,s'n^b \exp\left(-\frac{E}{k_B T}\right) \tag{13}$$

where s' is the general order preexponential factor, be represents the order of kinetics, and $s' = s$ for $b = 1$. Eq. (13) can be integrated

$$\int_{n_0}^{n}(n')^b = -\int s' \exp\left(-\frac{E}{k_B T}\right)dt \tag{14}$$

This has the solution

$$n^{1-b} = n_0^{1-b}\left[1 + \frac{s'(b-1)n_0^{b-1}}{q}\int_{T_i}^{T}\exp\left(-\frac{E}{k_B T'}\right)dT'\right]$$

or

$$n = n_0\left[1 + \frac{s'(b-1)n_0^{b-1}}{q}\int_{T_i}^{T}\exp\left(-\frac{E}{k_B T'}\right)dT'\right]^{\frac{1}{1-b}}$$

(15)

The intensity of Eq. (13) then becomes

$$I(T) = c\,s'\,\exp\left(-\frac{E}{k_B T}\right)n_0^b\left[1 + \frac{s'(b-1)n_0^{b-1}}{q}\int_{T_i}^{T}\exp\left(-\frac{E}{k_B T'}\right)dT'\right]^{\frac{b}{b-1}}$$

(16)

The maximum intensity of a peak occurs at temperature T_m. At this point, the derivative of the intensity is zero, as is the derivative of the logarithm of the intensity. Thus, we obtain at $T = T_m$ the relationship

$$\frac{d\{\ln[I(T)]\}}{dT}\bigg|_{T=T_m} = 0 = \frac{E}{k_B T_m^2} - \frac{b}{b-1}\left[1 + \frac{s'(b-1)n_0^{b-1}}{q}\int_{T_i}^{T}\exp\left(-\frac{E}{k_B T'}\right)dT'\right]^{-1}_{T=T_m}$$

$$\times\left(\frac{s'(b-1)n_0^{b-1}}{q}\exp\left(-\frac{E}{k_B T_m}\right)\right)$$

(17)

This yields

$$1 + \frac{s'(b-1)n_0^{b-1}}{q}\int_{T_i}^{T_m}\exp\left(-\frac{E}{k_B T}\right)dT = \frac{b\,s'\,n_0^{b-1}k_B T_m^2}{q\,E}\exp\left(-\frac{E}{k_B T_m}\right)$$

(18)

The following approximation can be made

$$\int_{T_i}^{T}\exp\left(-\frac{E}{k_B T'}\right)dT' \cong T\exp\left(-\frac{E}{k_B T}\right)\sum_{n=1}\left(\frac{k_B T}{E}\right)^n(-1)^{n-1}n!$$

(19)

which Kitis and Pagonis determined is usually "a very good numerical approximation" [69]. The series converges quickly, so only the first two terms need to be taken. Inserting Eq. (19) into (18) yields

$$1 + \frac{s'(b-1)n_0^{b-1}}{q}\left[T\exp\left(-\frac{E}{k_B T_m}\right)\left(\frac{kT}{E} - \frac{2k^2 T_m^2}{E^2}\right)\right] = \frac{b\,s'\,n_0^{b-1}k_B T_m^2}{qE}\exp\left(-\frac{E}{k_B T_m}\right),$$

which becomes

(20)

$$\frac{q\,E}{k_B T_m^2} = s'\,n_0^{b-1}\exp\left(-\frac{E}{k_B T_m}\right)\left[1 + (b-1)\frac{2k_B T_m}{E}\right]$$

At this point, we can calculate the first-order solutions for the method of two heating rates and the variable heating rate method by setting $b = 1$ and $s' = s$

$$\frac{q\,E}{k_B T_m^2} = s\exp\left(-\frac{E}{k_B T_m}\right) \tag{21}$$

Conducting a pair of TL measurements and recording the maximum temperature of a peak in both glow curves gives two such equations with different q and T_m, but with the same E and s. Division of one equation by the other gives

$$\frac{q_1 T_{m2}^2}{q_2 T_{m1}^2} = \exp\left(\frac{E}{k_B T_{m2}} - \frac{E}{k_B T_{m1}}\right) \tag{22}$$

which can be solved for E

$$E = \frac{k_B T_{m1} T_{m2}}{T_{m1} - T_{m2}}\ln\left(\frac{q_1 T_{m2}^2}{q_2 T_{m1}^2}\right) \tag{23}$$

which represents the activation energy to first-order kinetics using the method of two heating rates [2, 41, 65–66, 70]. The frequency factor can also be found by Eq. (21) once we have obtained E.

The variable heating rate method adapts the method of two heating rates to the case of many heating rates, to be solved graphically. From Eq. (12), for first-order kinetics

$$\ln\left(\frac{T_m^2}{q}\right) = E\left(\frac{1}{k_B T_m}\right) - \ln\left(\frac{s\,k_B}{E}\right) \tag{24}$$

Data can easily be plotted in this way to give the activation energy as its slope. **Figure 4** plots the data obtained from **Figure 2** for calculation of E and s using Eq. (24). Once E is calculated, s may be calculated from the y-intercept.

Activation energies calculated using the initial rise method, corrected initial rise method [63], and the method of variable heating rates is compared and presented in **Table 1**.

Note that the activation energies found for Peaks 2 and 3 match closely between the method of multiple heating rates and the corrected initial rise method and that the initial rise method in those peaks gives a significantly smaller result than the method of two heating rates. The latter point suggests that we may see the effects of retrapping proposed by Braunlich [62].

4.3. General order method of variable heating rates

The general order variable heating rate method and the method of multiple heating rates are as of yet poorly documented in the literature [2]. The solution of the general order variable heating rate method begins by taking the logarithm of Eq. (20)

$$\frac{E}{k_B T_m} = \ln\left\{\frac{s'\,n_0^{b-1}k_B T_m^2}{q\,E}\left[1 + (b-1)\frac{2k_B T_m}{E}\right]\right\}, \tag{25}$$

which can be separated into the parts

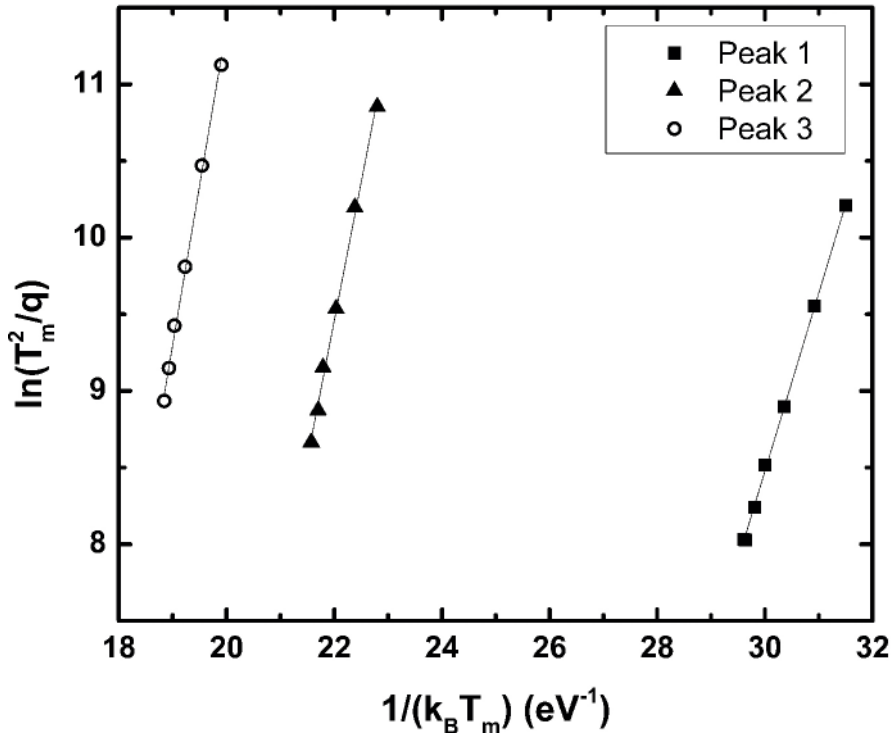## CeYAG 0.2% plot for determination of activation energies

Figure 4. Data and fits for all three peaks using multiple heating rates to get the results.

Peak 1 (470–720 nm, ~400 K)	Activation energy (eV)
Method of multiple heating rates	1.16 ± 0.01
Initial rise method	0.88 ± 0.06
Corrected initial rise	1.46 ± 0.05
Peak 2 (470–720 nm, ~550 K)	
Method of multiple heating rates	1.80 ± 0.05
Initial rise method	1.15 ± 0.06
Corrected initial rise	1.83 ± 0.10
Peak 3 (470–720 nm, ~600 K)	
Method of multiple heating rates	2.08 ± 0.05
Initial rise method	1.49 ± 0.07
Corrected initial rise	1.97 ± 0.05

Table 1. Calculated activation energies for the three major peaks found in Ce:YAG 0.2% thermoluminescence measurements from room temperature to 400°C using all methods previously discussed.

$$\frac{E}{k_B T_m} = \ln\left(\frac{T_m^2}{q}\right) + \ln\left[1 + (b-1)\frac{2k_B T_m}{E}\right] + \ln\left(\frac{s' \, n_0^{b-1} k_B}{E}\right) \tag{26}$$

The activation energy is typically at least an order of magnitude larger than $k_B T_m$ [2], so we can apply the series expansion for $\ln(1 + x)$ for $x \le 1$ to get

$$\ln\left(\frac{T_m^2}{q}\right) \approx \ln\left(\frac{E}{s' n_0^{b-1} k_B}\right) + \frac{E}{k_B T_m} - 2(b-1)\frac{k_B T_m}{E} + 2(b-1)^2\frac{k_B^2 T_m^2}{E^2} - \frac{8}{3}(b-1)^3\frac{k_B^3 T_m^3}{E^3} + \ldots \tag{27}$$

If we let $y = \ln(T_m^2/q)$ and $x = k_B T_m$ and designate y_0 as the logarithmic term independent of both q and T_m, Eq. (27) becomes

$$y = y_0 + \frac{E}{x} - 2(b-1)\frac{x}{E} + (b-1)^2\frac{x^2}{E^2} - \frac{8}{3}(b-1)^3\frac{x^3}{E^3} + \ldots \tag{28}$$

which can be plotted and fit using a simple fitting program. Mahesh et al. [2] solve this in a very different way:

$$\ln\left[I_m^{b-1}\left(\frac{T_m^2}{q}\right)^b\right] = b\ln E + \ln\left[\frac{(c \, s' \, n_0^{b-1})^{b-1}}{(s' \, b \, k_B)^b}\right] + \frac{E}{k_B T_m} \tag{29}$$

Eq. (29) shows dependence on intensity, which adds a further source of uncertainty. Detector zero drift, overlapping glow curve peaks, nonlinear intensity response by the detector, or other misleading intensity measurements will add error to calculations. Thus, Eq. (27) is preferred over Eq. (29) since it contains less factors that may create further sources of error.

The general order method of two heating rates can be solved by subtracting Eq. (27) for two different measurements

$$0 = \frac{E}{k_B}\left(\frac{1}{T_{m1}} - \frac{1}{T_{m2}}\right) + \ln\left(\frac{q_1 T_{m2}^2}{q_2 T_{m1}^2}\right) + \frac{2(b-1)k_B}{E}(T_{m2} - T_{m1}) - \frac{2(b-1)^2 k_B^2}{E^2}(T_{m2}^2 - T_{m1}^2)$$
$$+ \frac{8(b-1)^3 k_B^3}{3E}(T_{m2}^3 - T_{m1}^3) - \ldots \tag{30}$$

This is easiest solved graphically. After inputting all the known values for T_{mi} and q_i and the constants and letting $x = E$, we can write Eq. (30) as

$$y = Ax + B + \frac{C}{x} - \frac{D}{x^2} + \frac{E}{x^3} - \ldots \tag{31}$$

which can be plotted to find the x-intercept = E. The substitutions made are as follows:

$$A = \frac{1}{k_B}\left(\frac{1}{T_{m1}} - \frac{1}{T_{m2}}\right),$$

$$B = \ln\left(\frac{q_1 T_{m2}^2}{q_2 T_{m1}^2}\right),$$

$$C = 2(b-1)k_B(T_{m2}-T_{m1}), \tag{32}$$

$$D = 2(b-1)^2 k_B^2(T_{m2}^2 - T_{m1}^2),$$

$$E = \frac{8}{3}(b-1)^3 k_B^3(T_{m2}^3 - T_{m1}^3).$$

We may check our work here by setting $b = 1$ in Eq. (30), and we see that we return the first-order kinetics solution of Eq. (22).

The obvious challenge with this method, however, is the required guesswork for the order b.

The solution presented by Mahesh et al. [2] for the general order method of two heating rates is

$$\frac{T_{m1}^2}{q_1}\left(\frac{1}{b-1} + \frac{2k_B T_{m1}}{E}\right)\exp\left(-\frac{E}{k_B T_{m1}}\right) = \frac{T_{m2}^2}{q_2}\left(\frac{1}{b-1} + \frac{2k_B T_{m2}}{E}\right)\exp\left(-\frac{E}{k_B T_{m2}}\right) \tag{33}$$

which is not so easily solved for E and still requires inputting an assumed b. If $b = 1$, this can also be shown to return the first-order kinetics solution of Eq. (22).

Thus, we have formulated the theory for the initial rise method (Eq. 10), which can be applied to general order kinetics, the first-order method of two heating rates (Eq. 22) and variable heating rate method (Eq. 24), and general order method of two heating rates (Eq. 30) and variable heating rate method (Eq. 27).

5. Experimental setup

A schematic of a standard TL dosimetry reader (TLD) is shown in **Figure 5**. The irradiated dosimeter is mounted on a tray located within a readout chamber. Two different temperatures are used for heating the dosimeter, first one is preheating to clear noisy peaks and second one is readout temperature used to thermally stimulate the sample and collect data. Nitrogen gas is continuously pumped to decrease spurious phenomena [72] and reduce the background.

The absorbed dose is proportional to the output current received from photomultiplier tube [73].

We have developed an advanced TL setup that uses a special heating stage with an optical window that transmits light and blocks heat to achieve perfect temperature control during the measurement. Solarized fiber optics connected to collimation lenses are used to collect the emitted light (**Figure 6**). The TL spectra are recorded by a CCD detector with a 200 μm slit. The spectral range of the detector can be adjusted from 200 to 800 nm or from 350 to 1100 nm with 1 nm resolution. The optical components are water cooled to allow for high temperature
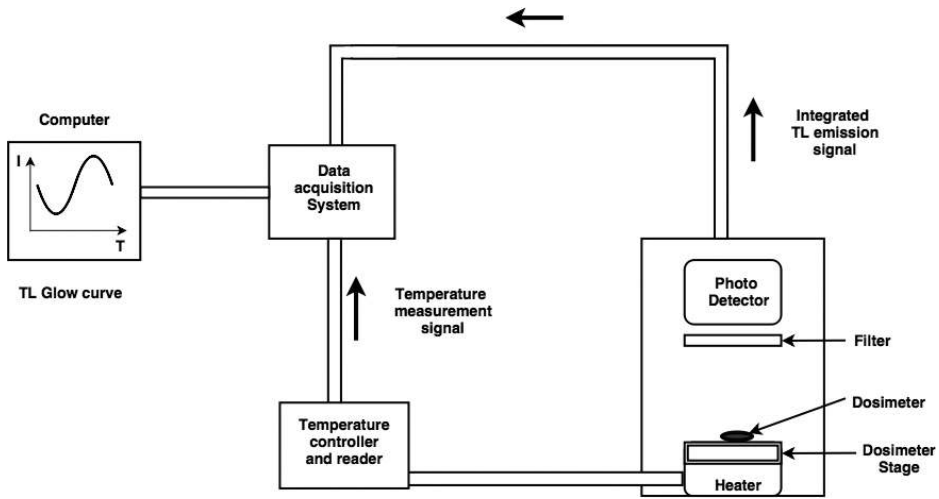
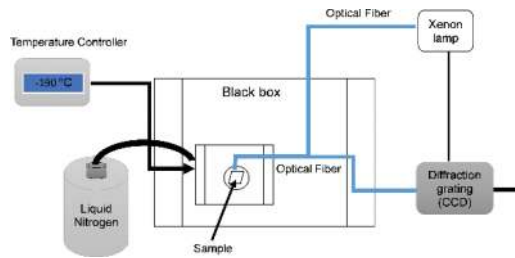**Figure 5.** Schematic of TLD reader setup [73].

Figure 6. Schematic diagram of a typical TL setup. The sample is heated on a heating stage at a constant rate and the frame temperature is regulated by a water pump. A collimated lens collect emitted light from the sample and carries it to a spectrometer.

(up to 400°C) TL measurements. Before TL experiment, we often irradiate the samples in dark for certain time using xenon lamp, light emitting diodes (LEDs), or 254 nm irradiation panel. The spectral range of the xenon lamp is 220–750 nm. This setup has many advantages including:

1. Precise control and measurements of temperature, 1 mK precision and high stability.

2. Adjustable heating/cooling rate, can go up to 1000°C/min. In most measurements, it is operated at 60°C/min and 120°C/min. Using different heating rates is required to calculate trap levels by variable heating rate methods.

3. TL can be measured as a function of temperature and wavelength simultaneously as shown in (**Figure 7**).
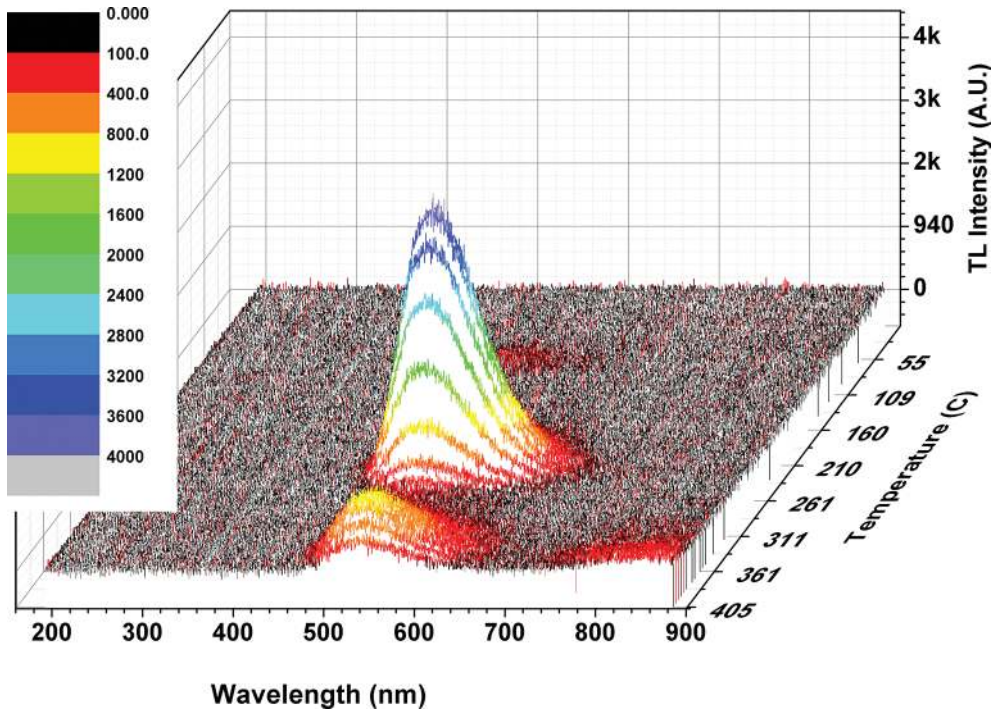
Figure 7. TL intensity versus temperature and wavelength.

A TL measurement is performed in a dark box in a temperature-insulated heating stage as discussed above and as shown in the figure. This is because the TL emission is relatively weak, so it is necessary to isolate the measurement from ambient lighting that would greatly interfere with it. The heating stage must be also temperature isolated for two reasons. First, it makes it possible to fully control the temperature of the sample instead of potentially creating a gradient of temperature across the thickness of the sample. Second, it separates the optical components used for excitation and measurement so that they may be operated independently.

6. TL applied to dielectrics

Dielectric materials possess a large band gap separating the valence and conduction bands. This large gap determines the characteristic insulating properties. Dopants, defects, and impurities alter the band structure of a dielectric material by adding energy levels and electron and electron hole traps within the band gap. Charge carrier traps can be vacancy, interstitial, substitutional, or antisite defects. Typically, charge carriers can be trapped at defects of the opposite charge. For instance, an anion vacancy is positively charged and would thus trap an electron. However, the behavior of some impurity traps depends on the electronic structure of

the impurity [74, 75]. For instance, in YAG, Eu^{3+}, and Yb^{3+} impurities have been found to act as stable electron traps at room temperature due to their large electron affinity. Meanwhile, Pr^{3+}, Tb^{3+}, and Ce^{3+} were found to act as hole traps, stable at room temperature [45, 57]. At low temperatures, other traps stabilize, such as Sm^{3+} electron traps.

TL can be used to characterize defects and provide quantitative information about charge carrier traps. It shares many similarities to color center measurements [76]; however, it has more advantages in evaluating the trap depths in the band gap. In color center measurements, a sample is irradiated for a period of time with an excitation source, similar to the first step for a TL measurement. Absorption spectra of this sample are recorded before and after excitation. As discussed previously, this excitation leads to the trapping of some charge carriers at defects. These trapped charge carriers carry their own optical properties, which are observable in absorption measurements. On top of that, an irradiated sample may be visibly discolored. Heating to sufficiently high temperature bleaches this discoloring and returns the trapped charge carriers to recombination centers. TL is the qualitative study of this effect. **Figure 8** shows the absorption spectra of undoped YAG before and after irradiation and after heating to 400°C. This sample will be also used later for TL glow curves presented in **Figure 12**. Some qualitative information can be gained from this figure in conjunction with prior knowledge about the sample, such as ascribing the peak at 256 nm to Fe impurities [77, 78]. These plots give no information about the depth of these traps other than the fact that heating to 400°C seemed to clear them up which implies that they are deep centers. TL provides the more qualitative analysis.

We will discuss our TL study on Ce:YAG as an example of dielectric materials because of its great importance in a wide range of applications from phosphors to scintillation. In general, YAG is one of the most important optical materials, with Nd:YAG as the most widely used laser crystal. As it stands now, Ce:YAG is an efficient luminescent material, but its performance as a scintillator is often hindered by the presence of traps.

6.1. YAG TL

In our TL measurements on YAG crystals [55], samples were cooled or heated within a temperature range of −190 to 400°C and TL spectra are recorded as described in the experimental section. Glow curves were constructed by integrating each spectrum over a specific range of wavelengths. In Ce-doped YAG, Ce ions provide the recombination centers and thus all TL emission are shown to have the luminescence profile characteristic of Ce ions in YAG, as shown in **Figure 9**. For the sake of demonstration, a contour plot of temperature versus wavelength for the same sample is provided in **Figure 10**, demonstrating only one luminescence center.

Sometimes care had to be taken when integrating over wavelengths to distinguish between different luminescence centers activating at different temperatures. **Figure 11** shows the contour plot of temperature versus wavelength for an undoped YAG sample, originally grown in a pure Ar atmosphere, where the luminescence centers are comprised of different trace impurities. Something else to note in **Figure 10** is the onset of IR emission near 400°C due to blackbody radiation. The wavelength of this IR emission overlapped slightly with the integration range of one of the peaks and was visible in the constructed glow curve. Also note the
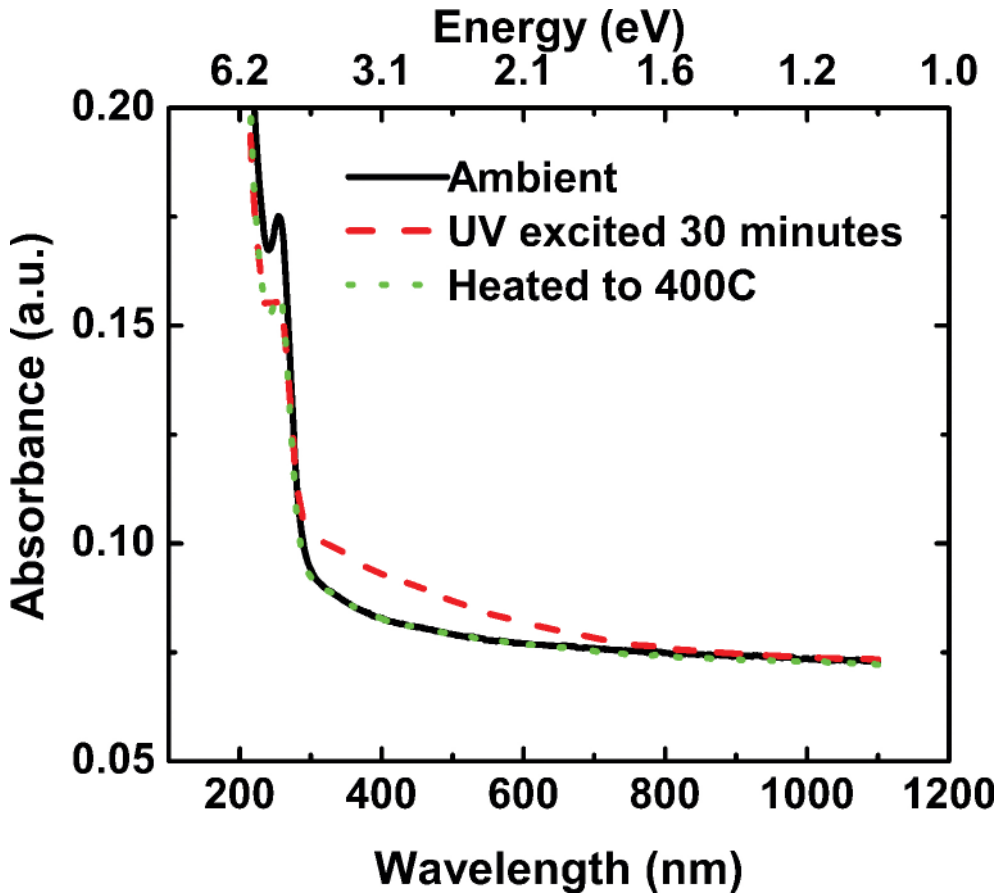
Figure 8. Air annealed Ar-grown YAG absorption spectra after UV excitation and heating.

much weaker emission, as each contour now corresponds to a step of 200 counts, whereas in **Figure 10**, it corresponded to 1500 counts. The IR radiation was too weak to show on the contour plot of **Figure 10**. The Ar-grown undoped YAG sample was annealed at 1200° for 96 hours in air. **Figure 12** presents the two unique glow curves for this sample before and after annealing, separately integrating over the wavelength ranges 340–570 and 570–800 nm. The intensity of most peaks has been decreased suggesting decreased concentration of their corresponding defects. Also, the high-temperature peak in the high-wavelength plot shifts significantly, suggesting a change in activation energy. Activation energies were calculated for each of these peaks and frequency factors were calculated whenever possible for the as-grown sample. The small peak in the high-wavelength glow curve at 180°C had too high of uncertainty to get a reliable estimate for s. Results are tabulated in **Tables 2** and **3**.

Obviously, the activation energy increases with temperature, as charge carriers at deeper traps require more thermal energy for release. The most noticeable change is the large decrease in
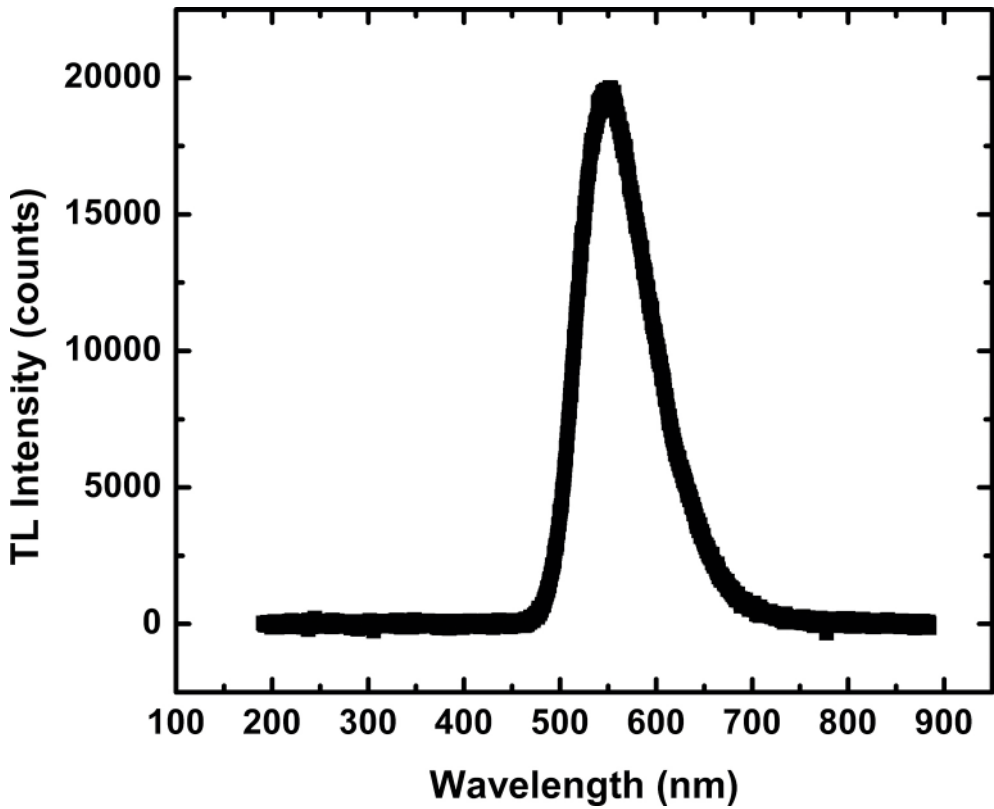
Figure 9. TL emission spectrum at 262°C for Ce:YAG 0.14%.

activation energy of the highest energy peak after annealing by about 0.9 eV. Due to the nature of anneal, it seems reasonable to attribute this defect partially to oxygen vacancies. However, the fact that the peak persists, just at a decreased activation energy, suggests that there still exists a defect, suggesting that the original defect was a complex defect consisting of both at least one Al vacancy and at least one O vacancy, and the anneal filled one O vacancy but left the Al vacancy. The depth of the low-wavelength peak at 250°C appears to decrease slightly after annealing, possibly due to the change in charge state of the impurity responsible for this luminescence and/or change of lattice defect structures surrounding them. No other activation energy appeared to change after annealing, so it would appear that annealing only decreased their concentration and not their depth.

Positron annihilation lifetime spectroscopy (PALS) measurements were also performed on these samples in combination with TL [79]. PALS works by injecting a positron into the crystal and timing how long it takes to annihilate with an electron within the sample. If the positron annihilates within the bulk of the sample, the process is very fast (of order 0.1 ns). If the positron becomes trapped at a vacancy or void, it takes longer to annihilate with an electron
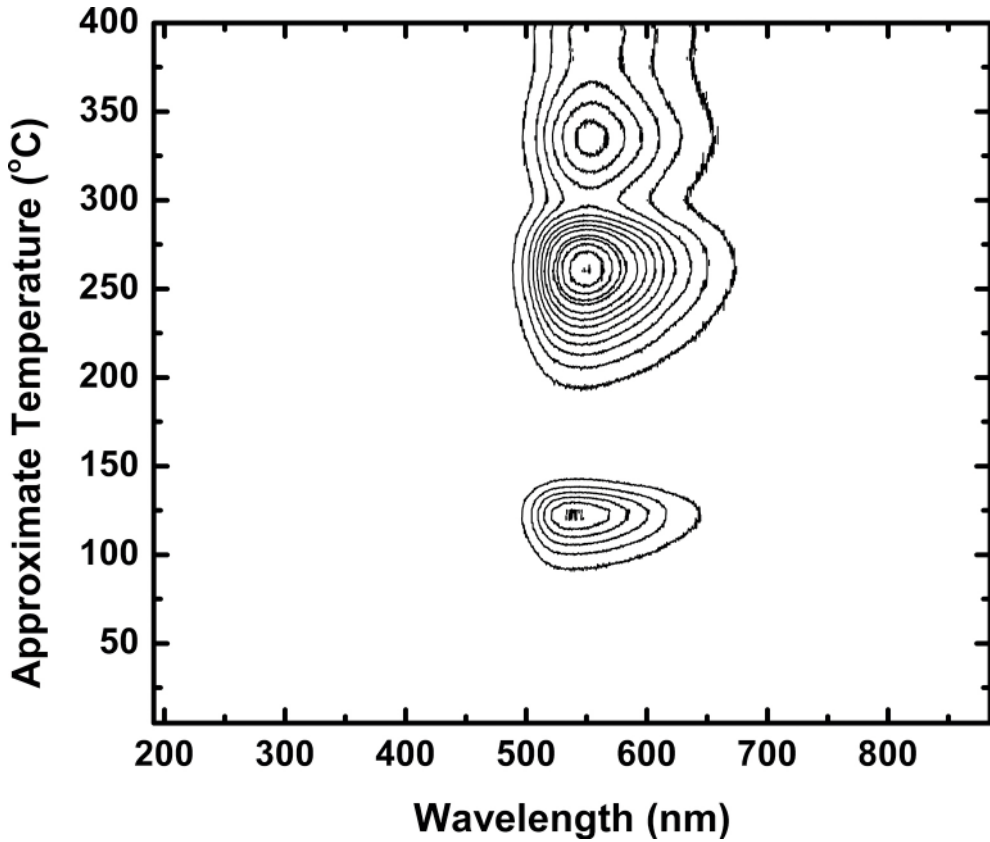
Figure 10. Contour plot of TL of Ce:YAG 0.14%, plotting luminescence intensity contours to a map of temperature versus wavelength. Each Contour represents 1500 counts [79].

due to the reduced number density of electrons at vacancies. Due to their positive charge, positrons typically trap at negatively charged vacancies or voids, such as cation vacancies, or neutral voids, such as cation + anion vacancy complexes. Typically, a larger vacancy means a lower number density of electrons and thus longer positron lifetime [80, 81].

PALS measurements on these YAG samples demonstrated a defect lifetime (i.e., the lifetime of a positron trapped at a defect) of 0.2931 ± 0.0032 ns for the as-grown sample and 0.2691 ± 0.0037 ns for the annealed sample, suggesting that annealing in air decreased the size of the defect but did not entirely eliminate it. This defect bears striking similarity to the peak in **Figure 12** that moved from 395 to 345°C after annealing in air and in fact the same conclusion may be drawn from this PALS result that this defect is due to an Al + O vacancy complex.

PALS measurements only identified one defect that trapped the injected positrons, suggesting that the remaining defects arose from either positively charged vacancies or nonvacancy
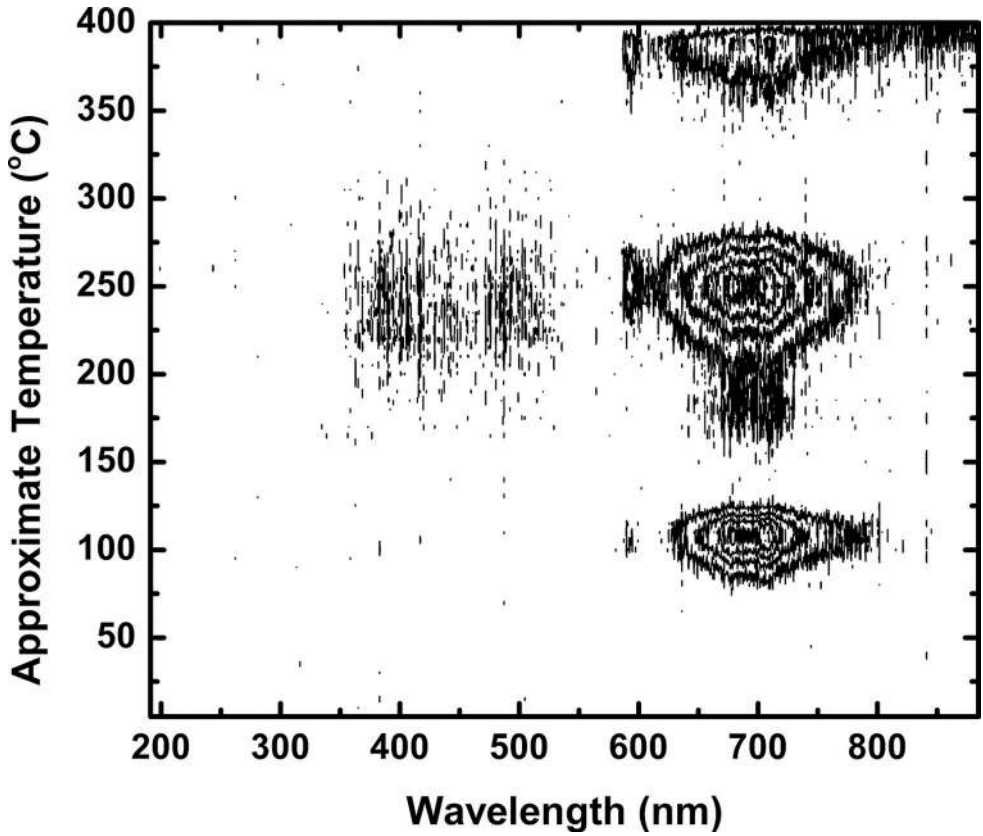
Figure 11. Contour plot of TL of undoped YAG grown in a pure Ar atmosphere, plotting luminescence intensity contours to a map of temperature versus wavelength. Each contour represents a step of 200 counts [79].
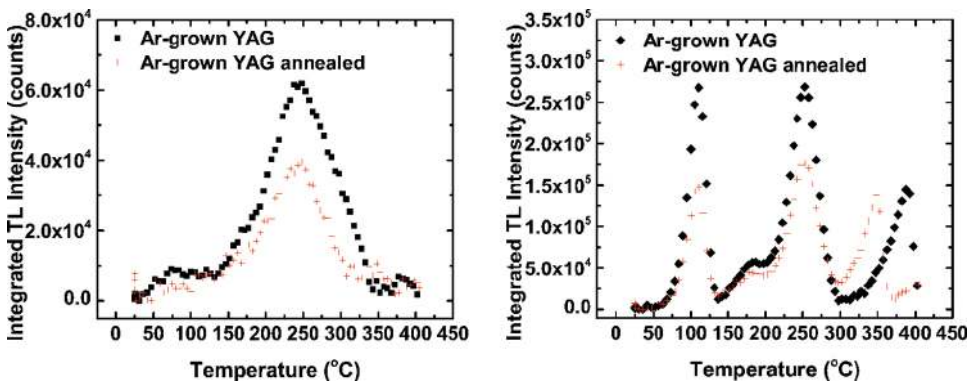

Figure 12. Glow curves for Ar-grown undoped YAG before and after annealing. The low wavelength curve (left) was integrated over 340–570 nm, the high wavelength curve (right) was integrated over 570–800 nm.

	Activation energy		Frequency factor
Approximate peak location (q = 60°C/min)	As grown	Air annealed	As grown
250°C	1.47 ± 0.23 eV	0.95 ± 0.09 eV	2.68 × 1010 s^{-1}

Table 2. Calculated activation energies of Ar-grown undoped YAG for the glow curves constructed using 340–570 nm integration.

	Activation energy		Frequency factor
Approximate peak location (q = 60°C/min)	As grown	Air annealed	As grown
110°C	1.65 ± 0.01 eV	1.63 ± 0.09 eV	6.47 × 1017 s^{-1}
180°C	3.04 ± 2.27 eV	1.44 ± 1.87 eV	(not calculated)
250°C	1.92 ± 0.09 eV	2.07 ± 0.15 eV	4.21 × 1019 s^{-1}
345°C	N/A	2.23 ± 0.55 eV	1.14 × 1022 s^{-1}
395°C	3.15 ± 0.25 eV	N/A	N/A

Table 3. Calculated activation energies of Ar-grown YAG for the glow curves constructed using 570–800 nm integration.

defects, such as impurities. Since a positively charged vacancy in this crystal means an O vacancy, annealing in air would be expected to eliminate or decrease this defect, and consequently any TL peaks associated with it. Other TL peaks that are not sensitive to air anneal can be ascribed to impurities.

6.2. Low-temperature TL of Ce:YAG

Low-temperature glow curves for Ce:YAG 0.14%, presented in **Figure 13**, provide an abundance of information. The sample was measured, then annealed in air for 48 hours at 1200°C and remeasured, then annealed in a vacuum for 24 hours at 800°C and measured once again. TL emission spectra were integrated over the wavelength range of 470–720 nm, which encompasses the strong and well-documented Ce luminescence peak in YAG peaked around 550 nm [51, 56, 57, 78, 82–106]. From figure, it can be seen that the highest intensity peak at −75°C is completely eradicated by annealing in air, but it returns after annealing in vacuum. With this information, it is easy to identify this trap as an oxygen vacancy. Upon eliminating this peak, TL emission can be distinguished near −100°C in the air-annealed sample. Curve fitting resolves that it is as two peaks centered at about −100 and −90°C. A weak peak at about −10°C appears to be eliminated by annealing in air.

Activation energies were calculated to compare the as-grown and air-annealed samples and are provided in **Table 4**. Interestingly, although all traps appear to decrease drastically in concentration, their depths uniformly increase.

These examples demonstrate some of the analytical capabilities of TL spectroscopy. The high-concentration oxygen vacancies observed in **Figure 13** at −75°C are not stable at room
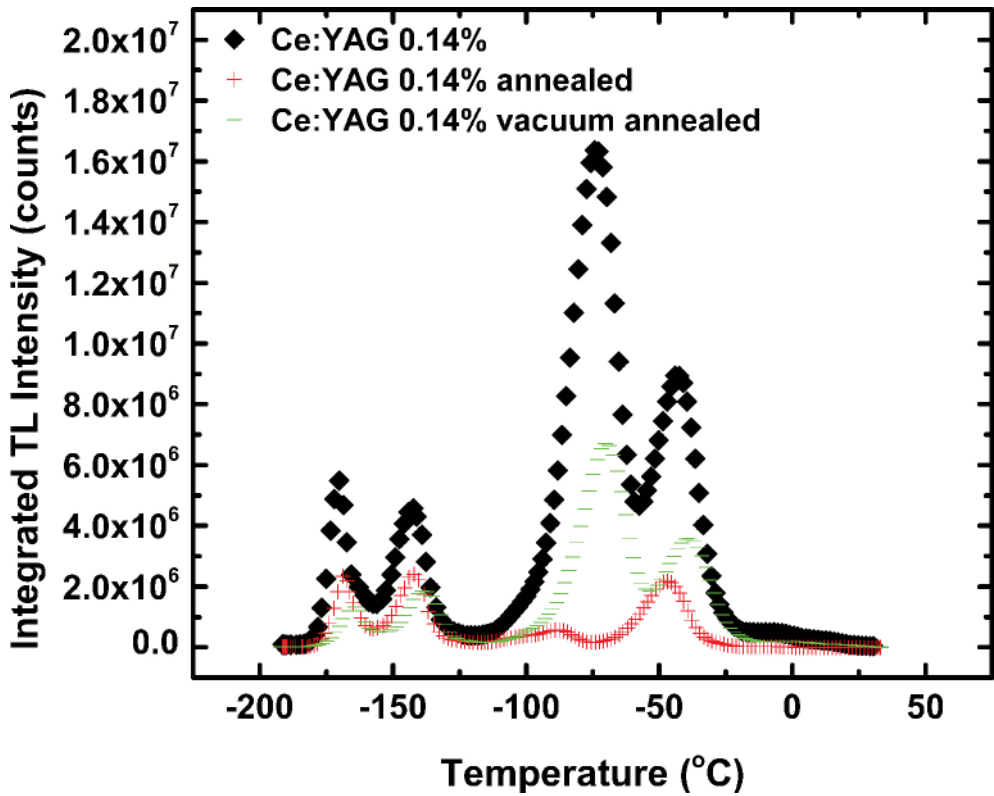
Figure 13. Low-temperature glow curves of Ce:YAG 0.14% as grown, annealed in air, and annealed in a vacuum using 470–720 nm integration.

	Activation energy	
Approximate peak location (q = 60°C/min)	As grown	Annealed in air
−170°C	0.20 ± 0.01 eV	0.37 ± 0.03 eV
−140°C	0.27 ± 0.01 eV	0.39 ± 0.02 eV
−100°C	N/A	0.38 ± 0.15 eV
−90°C	N/A	0.67 ± 0.06 eV
−75°C	0.55 ± 0.01 eV	N/A
−45°C	0.66 ± 0.01 eV	0.81 ± 0.01 eV
−10°C	0.90 ± 1.04 eV	N/A

Table 4. Calculated activation energies of Ce:YAG 0.14% for the glow curves constructed using 470–720 nm integration range.

temperature but would play a major role in any low-temperature processes involving Ce:YAG crystal. It also affects exciton dynamics in YAG crystal. It is clear how different processing affects the defect structure and concentration within these samples.

7. TL applied to semiconductors

7.1. Calculations of donor ionization energies in ZnO

In this section, we discuss a new application of TL that implies the use of low-temperature TL for the measurements of donor ionization energy in luminescent semiconductors. TL spectroscopy has been already applied in combination with other methods to identify defects in a few semiconductors as mentioned earlier in the chapter. However, the focus here is on its development as a method for donor ionization energy calculations. We have recently shown that it is possible to apply low-temperature TL to measure donor ionization energies in luminescent semiconductor. The study has been carried out on ZnO, one of the most important wide band gap semiconductors with many existing and future applications [107]. It is also considered one of the most
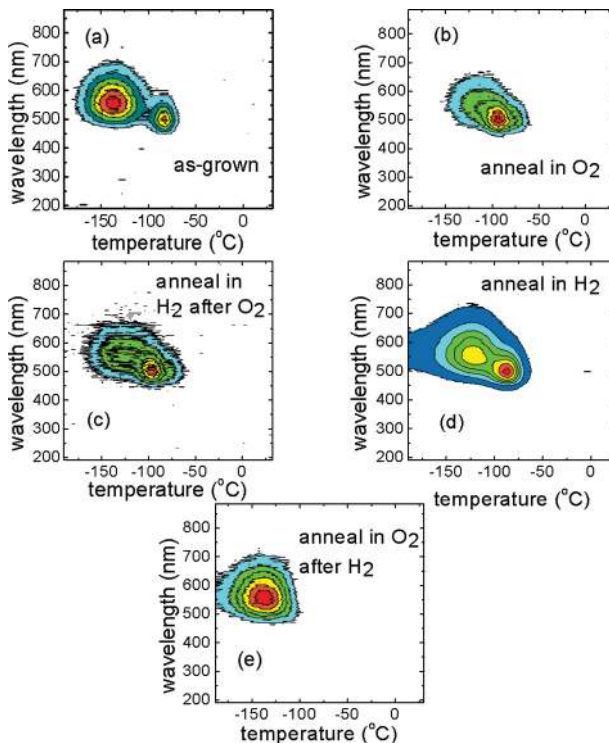

Figure 14. Contour plot of TL emission as a function of temperature and wavelength for as grown and annealed ZnO single crystals. 60°C/min was used for heating rate [116].

complex binary system in terms of defects and optoelectronic properties. There are several established methods for calculating donor and acceptor ionization energies in semiconductors. Temperature-dependent Hall-effect is the most common method, it is crucial for semiconductor characterization [108–110], however it suffers limitations in specific cases, and TL may provide an alternative method in these cases as explained below. Electron paramagnetic resonance (EPR) [110], and photoluminescence [111–115] have also been applied to measurements of donor ionization energies, however, EPR is very limited and PL alone may be not capable of measuring the donor ionization energy due to the collapse of exciton.

Low-temperature TL has been recently applied on as-grown and annealed ZnO single crystals [116]. Annealing was carried out in different atmospheres: (1) hydrogen atmosphere at 300°C for 1 hour. (2) Oxygen atmosphere at 1100°C for 1 hour. (3) Both atmospheres in different order. **Figure 14** represents the contour plots for as-grown and annealed samples, two peaks can be seen at 520 and 580 nm, which are slightly changed with the annealing atmospheres. **Figure 15** shows the glow curves for as-grown and annealed samples. Three donors were identified in the samples from the glow curves and their ionization energies were found to be 47 ± 3, 55 ± 5, and 36 ± 2 meV. The first two energies are in agreement with Lavrov [111, 112]
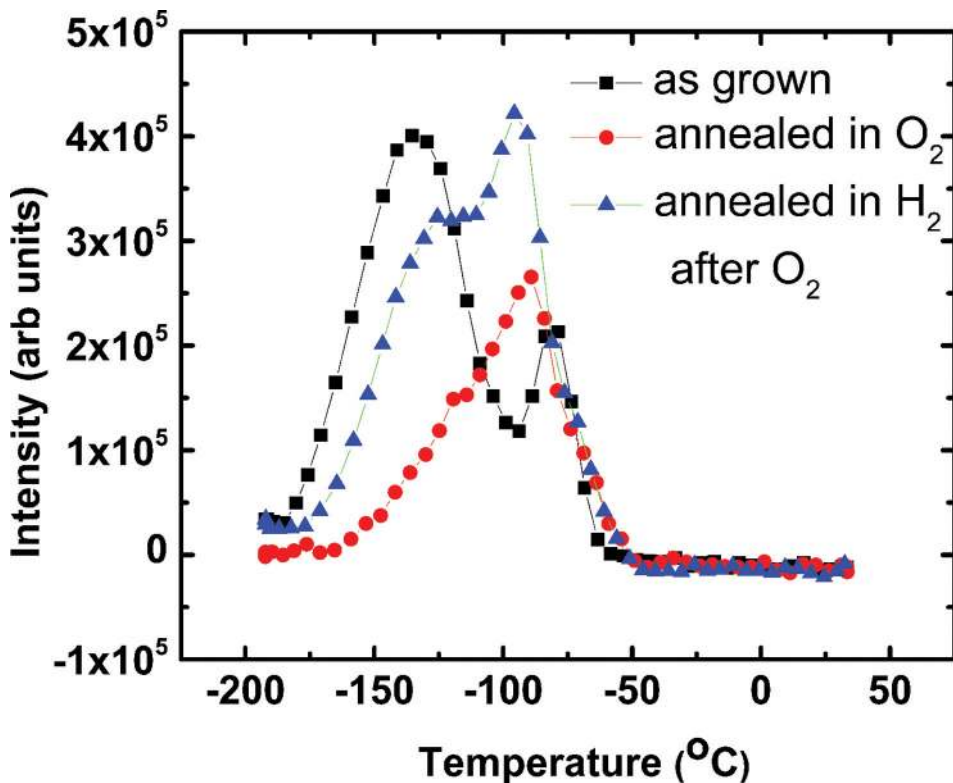

Figure 15. TL glow curve of ZnO single crystals produced from contour plots shown in **Figure 14 (a-c)** [116].

reports, the 47 meV was attributed to hydrogen bound in oxygen vacancy (H$_o$), and the 55 meV was related to hydrogen at a bound centered lattice site (H$_{BC}$). The 36 meV has also been reported for ZnO, and its origin is still in debate. **Figure 16** reveals the spectral range of TL emission that shows two peaks at 580 and 520 nm green luminescence centers, the ratio between them is dependent on the annealing conditions. The 580 nm emission peak is attributed to the Zn-O vacancy pairs which that have been modified after annealing in O$_2$ (**Figure 16b**). The 520 nm peak was reported as O-vacancy related defects, this peak was declined for the sample annealed in H$_2$ first and then annealed in O$_2$, where the 36 meV ionization energy has been measured. The reason behind it is that oxygen fills oxygen vacancies rather than Zn-O vacancies due to the formation of stable H-Zn vacancy complex defects, which supports the association of the 36 meV with "three or more hydrogen in Zn vacancy" donor. These TL measurements revealed the three known donors for ZnO in a single experiment, while each other method was only capable of measuring one type of the three donors. It should be noted that TL could be especially useful for small nonuniform samples because Hall-effect measurements require uniform sample and its resolution is limited to 5 × 5 mm.
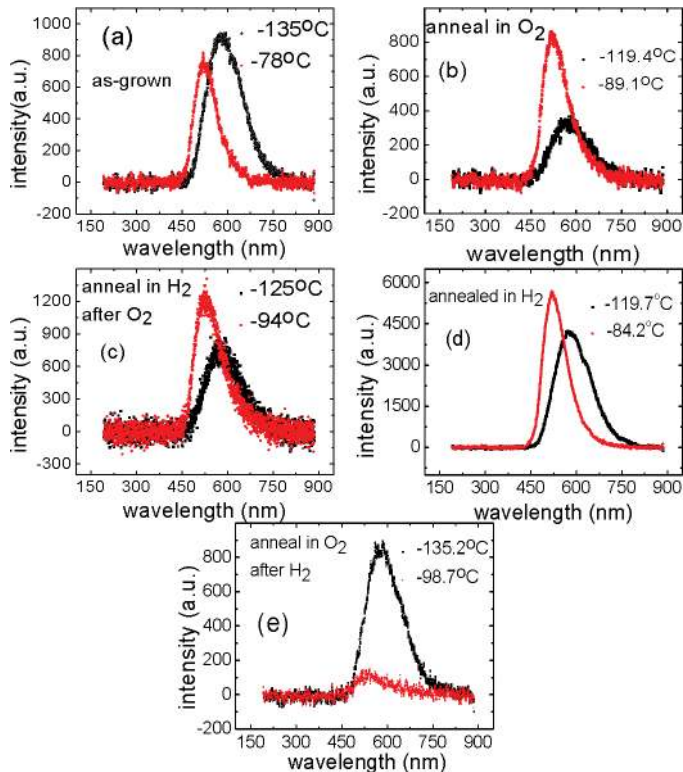

Figure 16. Emission peaks for as grown and annealed ZnO single crystals. Annealing atmosphere shows strong effects on the ratio of 580 and 520 nm [116].

Moreover, characterizing donors and acceptors in thin films on conductive layer using Hall-effect is a real challenge as the current diffuses to the conductive substrate and the measurements give a false indication for the electrical transport properties of the film. We expect that TL could be an alternative method for donor characterization in thin films on conductive layers

8. Conclusion

The chapter reviewed the basics of TL spectroscopy and its applications and described an advanced TL setup to extend its applications to the study and measurements of trap levels in semiconductors and dielectrics. Different methods for the analysis of TL glow curve and the calculations of activation energies were presented. By applying TL spectroscopy to the study of YAG and ZnO, we demonstrated the effectiveness of the technique in characterizing trap levels and measuring donor ionization energies in dielectrics and semiconductors, which is crucial to understand their electronic properties. By combining TL with other spectroscopies such as positron annihilation, Fourier transform infrared, and optical absorption spectroscopies, full characterization of trap levels in the band gap can be obtained. This is especially important for wide band gap materials where defects and dopants in the band gap determine most of the optical, electrical, and magnetic properties.

Author details

Pooneh Saadatkia[1], Chris Varney[2] and Farida Selim[1*]

*Address all correspondence to: faselim@bgsu.edu

1 Center for Photochemical Sciences, Bowling Green State University, Bowling Green, OH, USA

2 Seattle University, Seattle, WA, USA

References

[1] Harvey E. A history of luminescence. From early times until 1900. Baltimore, USA: The American Philosophical Society, JH Furst Co.; 1957.

[2] Mahesh K, Weng P, Furetta C. Thermoluminescence in solids and its applications. Ashford, Kent, England, UK: Nuclear Technology Pub.; 1989.

[3] Klingshirn CF. Semiconductor optics. Berlin: Springer Science & Business Media; 2012.

[4] Stokes GG. On the change of refrangibility of light. Philosophical Trans R Soc Lond 1852;142:463–562.

[5]   Valeur B, Berberan-Santos MN. A brief history of fluorescence and phosphorescence before the emergence of quantum theory. J Chem Educ 2011;88(6):731–738.

[6]   Selim FA. Luminescence based spectrometers. Patent 9261469; 2016.

[7]   Varney C, Khamehchi M, Ji J, Selim F. X-ray luminescence based spectrometer for investigation of scintillation properties. Rev Sci Instrum 2012;83(10):103112.

[8]   Chen R, McKeever SW. Theory of thermoluminescence and related phenomena. Singapore: World Scientific; 1997.

[9]   Dincer O, Ege A. Synthesis and luminescence of Tb 3 doped lithium borate (LiBO 2). J Lumin 2013;138:174–178.

[10] Kucuk N, Kucuk I, Cakir M, Keles SK. Synthesis, thermoluminescence and dosimetric properties of La-doped zinc borates. J Lumin 2013;139:84–90.

[11] Sharma S, Pitale S, Malik M, Dubey R, Qureshi M, Vasisth S, et al. Synthesis and thermoluminescence studies of Sr4Al14O25: Eu2 phosphor. Indian J Eng Mater Sci 2009;16 (3):165.

[12] Meijerink A, Blasse G. Photoluminescence and thermoluminescence properties of Ca2PO4Cl: Eu2. J Phys Cond Matt 1990;2(15):3619.

[13] Tanno H, Zhang S, Shinoda T, Kajiyama H. Characteristics of photoluminescence, thermoluminescence and thermal degradation in Eu-doped BaMgAl 10 O 17 and SrMgAl 10 O 17. J Lumin 2010;130(1):82–86.

[14] McKeever S, Moscovitch M, Townsend P. Thermoluminescence and thermoluminescence dosimetry. Thermoluminescence dosimetry materials: properties and uses. Ashford: Nuclear Technology Publishing; 1995:15–44.

[15] McKinlay AF. Thermoluminescence dosimetry.United Kingdom: Adam Hilger; 1981.

[16] McDougall DJ. Thermoluminescence of geological materials. London, new York: Academic Press; 1968.

[17] Aitken M. Physics and archaeology. Oxford, UK: Oxford University; 1974.

[18] Vij D. Thermoluminescent materials. New Jersey: Prentice Hall; 1993.

[19] Falcony C, Garcia M, Ortiz A, Alonso J. Luminescent properties of ZnS: Mn films deposited by spray pyrolysis. J Appl Phys 1992;72(4):1525–1527.

[20] McKeever SW. Thermoluminescence of solids. Cambridge: Cambridge University Press; 1988.

[21] Rasheedy M, Zahran E. The effect of the heating rate on the characteristics of some experimental thermoluminescence glow curves. Phys Scripta 2005;73(1):98.

[22] Shinsho K, Suzuki Y, Yamamoto Y, Urushiyama A. The thermoluminescence activation energy and frequency factor of the main glow of CaSO$_4$: Tm phosphor determined by

heating rate method including very slow rates of heating. J Appl Phys 2005;97 (12):3523.

[23] Dubey V, Tiwari R, Pradhan MK, Rathore GS, Sharma C, Tamrakar RK. Photoluminescece and thermoluminescence behavior of Zn2SiO4: Mn2, Eu2 Phosphor. J Lumin 2014;1(1):30–39.

[24] Sohn K, Cho B, Park HD. Excitation energy-dependent photoluminescence behavior in Zn 2 SiO 4: Mn phosphors. Mater Lett 1999;41(6):303–308.

[25] Zhang H, Buddhudu S, Kam C, Zhou Y, Lam Y, Wong K, et al. Luminescence of Eu 3 and Tb 3 doped Zn 2 SiO 4 nanometer powder phosphors. Mater Chem Phys 2001;68(1):31–35.

[26] Reinhard C, Gerner P, Garcí S, Valiente R, Güdel HU. Near-infrared to green photon upconversion in Mn 2 and Yb 3 doped lattices. Chem Phys Lett 2004;386(1):132–136.

[27] Taghavinia N, Lerondel G, Makino H, Yamamoto A, Yao T, Kawazoe Y, et al. Growth of luminescent Zn 2 SiO 4: Mn 2 particles inside oxidized porous silicon: emergence of yellow luminescence. J Cryst Growth 2002;237:869–873.

[28] Yamamoto H, Okamoto S, Kobayashi H. Luminescence of rare-earth ions in perovskite-type oxides: from basic research to applications. J Lumin 2002;100(1):325–332.

[29] Nalwa HS. Handbook of nanostructured materials and nanotechnology, five-volume set. San Diego, San Francisco, New York, Boston, London, Sydney, Tokyo: Academic Press; 1999.

[30] Lochab S, Pandey A, Sahare P, Chauhan R, Salah N, Ranjan R. Nanocrystalline MgB4O7: dy for high dose measurement of gamma radiation. Phys Status Solidi (a) 2007;204 (7):2416–2425.

[31] Lochab S, Sahare P, Chauhan R, Salah N, Ranjan R, Pandey A. Thermoluminescence and photoluminescence study of nanocrystalline Ba 0.97 Ca 0.03 SO4. Eur J Phys D 2007;40 (5):1343.

[32] Tiwari N, Kuraria RK, Tamrakar RK. Thermoluminescence glow curve for UV induced ZrO2:Ti phosphor with variable concentration of dopant and various heating rate. J Radiat Res Appl Sci 2014;7(4):542–549.

[33] Tamrakar RK, Bisen DP, Sahu IP, Brahme N. UV and gamma ray induced thermoluminescence properties of cubic Gd 2 O 3: Er 3 phosphor. J Radiat Res App Scie 2014;7 (4):417–429.

[34] Pathak P, Selot A, Kurchania R. Thermoluminescence properties of Mn-doped CaYAl 3 O 7 phosphor irradiated with ultra-violet, mega-voltage and gamma radiation. Radiat Phys Chem 2014;99:26–29.

[35] Baldacchini G, Chiacchiaretta P, Gupta V, Kalinov V, Voitovich A. Thermoluminescence, glow curves, and carrier traps in colored and nominally pure LiF crystals. Phys Sol Stat 2008;50(9):1747–1755.

[36] Tamrakar RK. Studies on absorption spectra of Mn doped Cds nanoparticles: lumines-cence study and absorption spectra of CdS: Mn. Saarbrücken: Lambert Academic Pub-lishing; 2012.

[37] Tamrakar RK, Bisen D. Optical and kinetic studies of CdS: Cu nanoparticles. Res Chem Intermed 2013;39(7):3043–3048.

[38] Tamrakar RK, Bisen D, Brahme N. Characterization and luminescence properties of Gd2O3 phosphor. Res Chem Intermediate 2014;40(5):1771–1779.

[39] Tamrakar RK, Bisen DP, Robinson CS, Sahu IP, Brahme N. Ytterbium doped gadolinium oxide (Gd 2 O 3: Yb 3). Indian J mat Sci 2014;2014:7 pages.

[40] Tamrakar RK. UV-irradiated thermoluminescence studies of bulk CdS with trap param-eter. Res Chem Intermediate 2015;41(1):43–48.

[41] Chen R, Kirsh Y. The analysis of thermally stimulated processes. Oxford: Pergamon press; 2013.

[42] Chen R, Lawless J, Pagonis V. A model for explaining the concentration quenching of thermoluminescence. Radiat Measur 2011;46(12):1380–1384.

[43] Chen R, Pagonis V. Thermally and optically stimulated luminescence: a simulation approach. New Jersey: John Wiley 2011.

[44] Bagdasarov KS, Pasternak L, Sevast'yanov B. Radiation color centers in Y3Al5O12: Cr3 tals. Sov J Quant Electron 1977;7(8):965.

[45] Batygov SK, Radyukhi VS, Maier A, Denker B, Timoshec MI, Voronko Y, et al. Color centers in Y3Al5O12 crystals. Fizika Tverdogo Tela 1972;14(4):977.

[46] Guerassimova N, Dujardin C, Garnier N, Pedrini C, Petrosyan A, Kamenskikh I, et al. Charge-transfer luminescence and spectroscopic properties of Yb 3 in aluminium and gallium garnets. Nucl Instr Methods Phys Res A Accelerat Spectromet Detectors Assoc Equip 2002;486(1):278–282.

[47] Mackay D, Varney C, Buscher J, Selim F. Study of exciton dynamics in garnets by low temperature thermo-luminescence. J Appl Phys 2012;112(2):023522.

[48] Milliken E, Oliveira L, Denis G, Yukihara E. Testing a model-guided approach to the development of new thermoluminescent materials using YAG: Ln produced by solution combustion synthesis. J Lumin 2012;132(9):2495–2504.

[49] Mori K. Transient colour centres caused by UV light irradiation in yttrium aluminium garnet crystals. Phys Status Solidi (a) 1977;42(1):375–384.

[50] Murk V, Yaroshevich N. Exciton and recombination processes in YAG crystals. J Phys Condens Matt 1995;7(29):5857.

[51] Robbins D, Cockayne B, Glasper J, Lent B. The temperature dependence of rare-earth activated garnet phosphors I. Intensity and lifetime measurements on undoped and Ce-doped. J Electrochem Soc 1979;126(7):1213–1220.

[52] Selim F, Solodovnikov D, Weber M, Lynn K. Identification of defects in Y3Al5O12 crystals by positron annihilation spectroscopy. Appl Phys Lett 2007;91(10):4105.

[53] Smol'Skaya L, Martynovich E, Davydchenko A, Smirnova S. X-ray and thermally stimulated luminescence in YAG. J App Spectrosc 1987;46(1):44–46.

[54] Solodovnikov D, Weber M, Lynn K. Improvement in scintillation performance of Ce, Er codoped yttrium aluminum garnet crystals by means of a postgrowth treatment. Appl Phys Lett 2008;93(10):104102.

[55] Varney C, Mackay D, Pratt A, Reda S, Selim F. Energy levels of exciton traps in yttrium aluminum garnet single crystals. J Appl Phys 2012;111(6):063505.

[56] Vedda A, Di Martino D, Martini M, Mares J, Mihokova E, Nikl M, et al. Trap levels in Y-aluminum garnet scintillating crystals. Radiat Measur 2004;38(4):673–676.

[57] Zorenko Y, Zorenko T, Gorbenko V, Voznyak T, Savchyn V, Bilski P, et al. Peculiarities of luminescent and scintillation properties of YAG: Ce phosphor prepared in different crystalline forms. Optical Mat 2012;34(8):1314–1319.

[58] Zych E, Brecher C, Glodo J. Kinetics of cerium emission in a YAG: Ce single crystal: the role of traps. J Phys Condens Matter 2000;12(8):1947.

[59] Randall J, Wilkins M. The phosphorescence of various solids. Proc Royal Soc London A Math Phys Sci 1945;184(999):347–364.

[60] Randall J, Wilkins M. Phosphorescence and electron traps. I. The study of trap distributions. Proc Royal Soc London A Math Phys Eng Sci Royal Soc 1945;184:365-389.

[61] Randall J, Wilkins M. Phosphorescence and electron traps. II. The interpretation of long-period phosphorescence. Proc Royal Soc London A Math Phys Eng Sci Royal Soc 1945;184:390-407

[62] Bräunlich P. Comment on the initial-rise method for determining trap depths. J Appl Phys 1967;38(6):2516–2519.

[63] Christodoulides C. Errors involved in the determination of activation energies in TL and TSDC by the initial rise method. J Phys D 1985;18(8):1665.

[64] Garlick G, Gibson A. The electron trap mechanism of luminescence in sulphide and silicate phosphors. Proc Phys Soc 1948;60(6):574.

[65] Bos A. High sensitivity thermoluminescence dosimetry. Nucl Instrum Methods Phys Res B 2001;184(1):3–28.

[66] Kitis G, Tuyn J. A simple method to correct for the temperature lag in TL glow-curve measurements. J Phys D 1998;31(16):2065.

[67] Pankove JI. Optical processes in semiconductors. New York: Dover publications; 2012.

[68] Devault D, Govindjee, Arnold W. Energetics of photosynthetic glow peaks. Proc Natl Acad Sci U S A 1983;80(4):983–987.

[69] Kitis G, Pagonis V. Peak shape methods for general order thermoluminescence glow-peaks: a reappraisal. Nucl Instrum Methods Phys Res B 2007;262(2):313–322.

[70] Kitis G, Gomez-Ros J, Tuyn J. Thermoluminescence glow-curve deconvolution functions for first, second and general orders of kinetics. J Phys D 1998;31(19):2636.

[71] May C, Partridge J. Thermoluminescent kinetics of alpha-irradiated alkali halides. J Chem Phys 1964;40(5):1401–1409.

[72] Grandfond A, Gautier B, Militaru L, Albertini D, Descamps-Mandine A. Spurious phenomena occurring during current measurement on ultra-thin dielectric layers: from electro-thermal effects to surface damage. J Appl Phys 2014;115(13):134103.

[73] VanDam J, Marinello G. Methods for in vivo dosimetry in external radiotherapy. Belgium: Garant Publ.; 1994.

[74] Winarski D, Persson C, Selim F. Hydrogen in insulating oxide Y3Al5O12 strongly narrows the band gap. Appl Phys Lett 2014;105(22):221110.

[75] Reda S, Varney C, Selim F. Radio-luminescence and absence of trapping defects in Nd-doped YAG single crystals. Res Phys 2012;2:123–126.

[76] Varney CR, Selim FA. Color centers in YAG. AIMS Mater Sci 2015;2(4):560–572.

[77] Varney C, Reda S, Mackay D, Rowe M, Selim F. Strong visible and near infrared luminescence in undoped YAG single crystals. AIP Adv 2011;1(4):042170.

[78] Varney C, Mackay D, Reda S, Selim F. On the optical properties of undoped and rare-earth-doped yttrium aluminium garnet single crystals. J Phys D 2011;45(1):015103.

[79] Varney C, Selim F. Positron lifetime measurements of vacancy defects in complex oxides. Acta Phys Polonica A 2014;125(3):764–766.

[80] Selim F, Varney C, Tarun M, Rowe M, Collins G, McCluskey M. Positron lifetime measurements of hydrogen passivation of cation vacancies in yttrium aluminum oxide garnets. Phys Rev B 2013;88(17):174102.

[81] Selim F, Winarski D, Varney C, Tarun M, Ji J, McCluskey M. Generation and characterization of point defects in SrTiO 3 and Y 3 Al 5 O 12. Results Phys 2015;5:28–31.

[82] Babin V, Laguta V, Maaroos A, Makhov A, Nikl M, Zazubovich S. Luminescence of F-type centers in undoped Lu3Al5O12 single crystals. Physica Status Solidi (b) 2011;248 (1):239–242.

[83] Baciero A, Placentino L, McCarthy K, Barquero L, Ibarra A, Zurro B. Vacuum ultraviolet and x-ray luminescence efficiencies of Y3Al5O12: Ce phosphor screens. J Appl Phys 1999;85(9):6790–6796.

[84] Blasse G, Bril A. A new phosphor for flying-spot cathode-ray tubes for color television: yellow-emitting Y3Al5O12–Ce3. Appl Phys Lett 1967;11(2):53–55.

[85] Blasse G, Bril A. Investigation of some Ce3-activated phosphors. J Chem Phys 1967;47 (12):5139–5145.

[86] Blazek K, Krasnikov A, Nejezchleb K, Nikl M, Savikhina T, Zazubovich S. Luminescence and defects creation in Ce3-doped Lu3Al5O12 crystals. Phys Status Solidi (b) 2004;241 (5):1134–1140.

[87] Dong Y, Zhou G, Jun X, Zhao G, Su F, Su L, et al. Luminescence studies of Ce: YAG using vacuum ultraviolet synchrotron radiation. Mater Res Bull 2006;41(10):1959–1963.

[88] Fagundes-Peters D, Martynyuk N, Lünstedt K, Peters V, Petermann K, Huber G, et al. High quantum efficiency YbAG-crystals. J Lumin 2007;125(1):238–247.

[89] Gibbons E, Tien T, Delosh R, Zacmanidis P, Stadler H. Some factors influencing the luminous decay characteristics of Y 3Al5 O 12: Ce3. J Electrochem Soc 1973;120(6):835–837.

[90] Hamilton D, Gayen S, Pogatshnik G, Ghen R, Miniscalco W. Optical-absorption and photoionization measurements from the excited states of Ce 3: Y 3 Al 5 O 12. Phys Rev B 1989;39(13):8807.

[91] Kirm M, Lushchik A, Lushchik C, Zimmerer G. Investigation of luminescence properties of pure and Ce3+ doped Y3Al5O12 crystals using VUV radiation. Electrochem Soc Proc 1999; 99–40:113-22.

[92] Liu B, Gu M, Liu X, Huang S, Ni C. Formation energies of antisite defects in Y3Al5O12: a first-principles study. Appl Phys Lett 2009;94(12):121910.

[93] Meng JX, Li JQ, Shi ZP, Cheah KW. Efficient energy transfer for Ce to Nd in Nd/Ce codoped yttrium aluminum garnet. Appl Phys Lett 2008;93(22):1908.

[94] Miniscalco W, Pellegrino J, Yen W. Measurements of excited-state absorption in Ce3: YAG. J Appl Phys 1978;49(12):6109–6111.

[95] Moszyński M, Ludziejewski T, Wolski D, Klamra W, Norlin L. Properties of the YAG: Ce scintillator. Nucl Instrum Methods Phys Res A 1994;345(3):461–467.

[96] Pedrini C, Rogemond F, McClure D. Photoionization thresholds of rare-earth impurity ions. Eu2: CaF2, Ce3: YAG, and Sm2: CaF2. J Appl Phys 1986;59(4):1196–1201.

[97] Pédrini C. Electronic processes in rare earth activated wide gap materials. Phys Status Solidi (a) 2005;202(2):185–194.

[98] Robbins D, Cockayne B, Lent B, Duckworth C, Glasper J. Investigation of competitive recombination processes in rare-earth activated garnet phosphors. Phys Rev B 1979;19 (2):1254.

[99] Robbins D, Cockayne B, Glasper J, Lent B. The temperature dependence of rare-earth activated garnet phosphors II. A comparative study of Ce3, Eu3, Tb3, and Gd3. J Electrochem Soc 1979;126(7):1221–1228.

[100] Rotman S, Tuller H, Warde C. Defect-property correlations in garnet crystals. VI. The electrical conductivity, defect structure, and optical properties of luminescent calcium and cerium-doped yttrium aluminum garnet. J Appl Phys 1992;71(3):1209–1214.

[101] Suzuki Y, Sakuma T, Hirai M. UV emission from the second lowest 5d state in Ce3: YAG. Mater Sci Forum 1997;239–241:219–222.

[102] Tomiki T, Akamine H, Gushiken M, Kinjoh Y, Miyazato M, Miyazato T, et al. Ce3 centres in Y3Al5O12 (YAG) single crystals. J Physic Soc Japan 1991;60(7):2437–2445.

[103] Zorenko Y, Voloshinovskii A, Savchyn V, Voznyak T, Nikl M, Nejezchleb K, et al. Exciton and antisite defect-related luminescence in Lu3Al5O12 and Y3Al5O12 garnets. Phys Status Solidi (b) 2007;244(6):2180–2189.

[104] Zorenko Y, Mares J, Prusa P, Nikl M, Gorbenko V, Savchyn V, et al. Luminescence and scintillation characteristics of YAG: Ce single crystalline films and single crystals. Radiat Measur 2010;45(3):389–391.

[105] Zorenko Y, Voznyak T, Gorbenko V, Zych E, Nizankovski S, Dan'Ko A, et al. Luminescence properties of Y 3 Al 5 O 12: Ce nanoceramics. J Lumin 2011;131(1):17–21.

[106] Zych E, Brecher C, Glodo J. Kinetics of cerium emission in a YAG: Ce single crystal: the role of traps. J Phys 2000;12(8):1947.

[107] Selim F, Tarun M, Wall D, Boatner LA, McCluskey M. Cu-doping of ZnO by nuclear transmutation. Appl Phys Lett 2011;99(20):202109.

[108] Look DC, Hemsky JW, Sizelove J. Residual native shallow donor in ZnO. Phys Rev Lett 1999;82(12):2552.

[109] Look DC, Reynolds DC, Sizelove J, Jones R, Litton CW, Cantwell G, et al. Electrical properties of bulk ZnO. Solid State Commun 1998;105(6):399–401.

[110] Hofmann DM, Hofstaetter A, Leiter F, Zhou H, Henecker F, Meyer BK, et al. Hydrogen: a relevant shallow donor in zinc oxide. Phys Rev Lett 2002;88(4):045504.

[111] Lavrov E, Herklotz F, Weber J. Identification of two hydrogen donors in ZnO. Phys Rev B 2009;79(16):165210.

[112] Lavrov E. Hydrogen in ZnO. Phys B Condens Matt 2009;404(23):5075–5079.

[113] Meyer B, Sann J, Hofmann D, Neumann C, Zeuner A. Shallow donors and acceptors in ZnO. Semicond Sci Tech 2005;20(4):S62.

[114] Meyer B, Alves H, Hofmann D, Kriegseis W, Forster D, Bertram F, et al. Bound exciton and donor–acceptor pair recombinations in ZnO. Phys Status Solidi (b) 2004;241(2):231–260.

[115] Schildknecht A, Sauer R, Thonke K. Donor-related defect states in ZnO substrate material. Phys B Condens Matt 2003;340:205–209.

[116] Ji J, Boatner L, Selim F. Donor characterization in ZnO by thermally stimulated luminescence. Appl Phys Lett 2014;105(4):041102.